Supplemental Document

Optics EXPRESS

Time-dependent Monte Carlo modeling of fluorescent optical antennas for optical wireless communication: supplement

SANDRA DORIA,[1,4,*] MAURO ARESTI,[2,4] MARCO MEUCCI,[2,4] MARIANGELA DI DONATO,[1,4] MASSIMO CALAMANTE,[1,5] DANIELE FRANCHI,[1] ANDREA PUCCI,[1,6] ANTONELLA BATTISTI,[7] MARCO FATTORI,[3,4] AND JACOPO CATANI[2,4]

[1]*Institute for Chemistry of Organometallic Compounds (CNR-ICCOM), Via Madonna del Piano 10, I-50019, Sesto Fiorentino, Italy*
[2]*National Institute of Optics (CNR-INO), Via Nello Carrara 1, I-50019, Sesto Fiorentino, Italy*
[3]*Physics and Astronomy department, via Giovanni Sansone 1, I-50019 Sesto Fiorentino, Italy*
[4]*European Laboratory for Non Linear Spectroscopy (LENS), Via Nello Carrara 1, I-50019, Sesto Fiorentino, Italy*
[5]*Department of Chemistry "Ugo Schiff", University of Florence, via della Lastruccia 13, 50019 Sesto Fiorentino, Italy*
[6]*Department of Chemistry and Industrial Chemistry, University of Pisa, via Moruzzi 13, 56124 Pisa, Italy*
[7]*Nanoscience Institute–CNR, NEST-SNS, Piazza San Silvestro 12, I-56127 Pisa, Italy*
[*]*doria@lens.unifi.it*

Supplement DOI: https://doi.org/10.6084/m9.figshare.32672358

Parent Article DOI: https://doi.org/10.1364/OE.601352

Time-dependent Monte Carlo simulation of fluorescent Optical Antennas for Optical Wireless Communication: Supplement 1

1. EXPERIMENTAL METHOD

A. Preparation of Fluorescent Concentrators

PMMA slabs doped with the DQ1 and LR305 fluorophores were prepared by cell casting according to the following procedure: Free-radical polymerization of methyl methacrylate was carried out by pouring a solution containing methyl methacrylate (MMA, 40.0 g, 80 wt%), poly(methyl methacrylate) (10.0 g, 20 wt%), the fluorophores (DQ1 or LR305) at the desired concentrations (200, 300, 400, 500, 750, and 1000 ppm), and 2,2′-Azobisisobutyronitrile (AIBN, 0.30 g, 0.1 wt%) as the radical initiator into a $15 \times 15 \times 0.3\text{cm}^3$ mold. The molds were assembled from two glass plates separated by an elastic PVC gasket and secured with metallic clamps. The gasket thickness exceeded that of the target Fluorescent Concentrators (FCs), thereby ensuring the correct sheet thickness under the pressure exerted by the clamps. The sealed mold was placed in a water-filled bath at 50 ^{o}C overnight and subsequently transferred to an oven for 4 h of curing at 120 ^{o}C. Upon completion of the curing process, the glass plates were separated, and the resulting PMMA slab was laser-cut to the required dimensions and polished.

B. Spectroscopy characterization

Fluorescence spectra were recorded with a Perkin Elmer LS55 spectrofluorimeter. In this setup, the excitation beam is tightly focused on a small volume of the sample, and the emitted light is collected in a geometry designed to minimize the optical path within the fluorophore. This configuration reduces the likelihood of reabsorption, ensuring that the measured spectra accurately reflect the intrinsic emission of the sample without distortions from photons being reabsorbed and re-emitted. Fluorescence quantum yield (QY) was measured by means of a Jasco FP-8300, instrument equipped with a 100 mm-diameter integrating sphere ILF-835. The slight variation in QY with concentration can be explained by different PMMA micro-environments or formation of microaggregates (dimers, excimers).

C. Microscopy imaging and FLIM

The full characterization of the two FCs series included microscope imaging in order to assess the presence of aggregates, especially at high dye concentration, and to determine the fluorescence lifetime. Fluorescence lifetime imaging microscopy (FLIM) was performed using a Leica TCS SP5 inverted laser scanning confocal microscope equipped with an external pulsed diode laser for time-correlated single-photon counting (TCSPC). The system was configured with either a 63×/1.4 NA water-immersion objective or a 100×/1.3 NA oil-immersion objective (Leica). Pulsed excitation (wavelength 405 or 470 nm) was achieved using diode laser lines appropriate for the fluorophores of interest, allowing precise temporal resolution necessary for fluorescence lifetime measurements. Photon arrival times were recorded and fluorescence decay curves were reconstructed for each pixel, and lifetimes were extracted using exponential fitting algorithms.

No significant aggregation was observed in either LR305- or DQ1-doped PMMA FCs within the optical resolution limit of the microscope.

For LR305, time-resolved measurements were performed using a 40 MHz repetition rate. The fluorescence decay curves were well fitted with a mono-exponential function, yielding a single lifetime component independent of dye concentration, supporting the hypothesis of the absence of aggregation. Repeated acquisitions in different regions of the samples produced consistent fitting parameters, with an average lifetime of 5.3 ns. These results indicate that LR305 exhibits uniform photophysical behavior within the PMMA matrix across the investigated concentration range.

For DQ1, however, non-negligible residuals for mono-exponential fit suggested the need for further investigation: measurements at both 40 MHz and 20 MHz repetition rates confirmed the need for a bi-exponential model, with an average lifetime of 6.7 ns, independent of concentration. Interestingly, the relative contributions of the two populations—expressed as the ratio of the pre-exponential weights—were found to depend on dye concentration. This observation may indicate the presence of microaggregates (e.g., dimers or excimers) that were not resolved by microscopy imaging, or local variations in the polymer microenvironment affecting the fluorescence dynamics.

Representative time-decay curves along with the corresponding fitting functions are presented in Figure S1, and a summary of the extracted fit parameters is reported in Table S1.

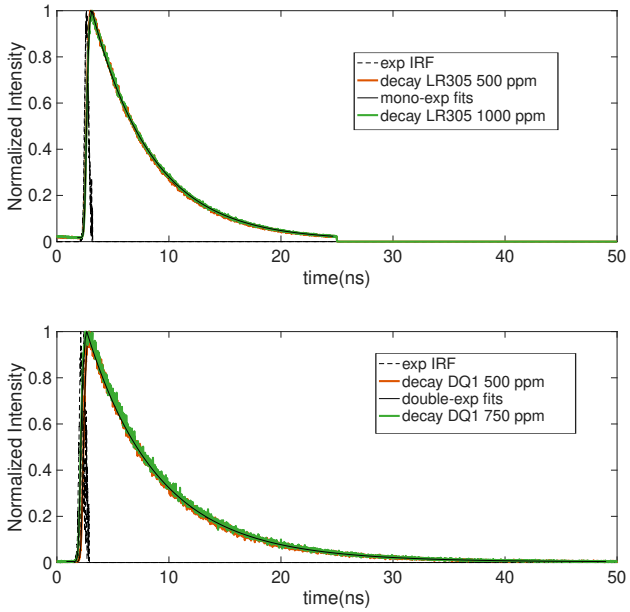

Fig. S1. Representative fluorescence lifetime decay curves acquired by FLIM for LR305- (top) and DQ1-doped (bottom) luminescent solar concentrators. Experimentally measured TCSPC decays are shown together with the instrument response function (IRF) and the corresponding fitting functions. LR305 data, acquired at a 40 MHz repetition rate, are well described by a mono-exponential decay, indicating a single emissive population. In contrast, DQ1 measurements, acquired at 20 MHz, require a bi-exponential fit, revealing the presence of two distinct lifetime components.

D. Physical characterization

The physical thickness of each FC sample was measured using a digital caliper with a precision of ±0.01 mm. The thickness measurements were used as geometric constraints in the Monte Carlo ray-tracing simulations to ensure accurate modeling of photon propagation within each specific device geometry.

E. OAs characterization for Monte Carlo validation

The OAs were constructed by optically coupling the FCs to different photodetectors for each measurement. Specifically, a fast APD430 from Thorlabs (active area diameter: 0.5 mm) with a bandwidth of 400 MHz was chosen for the rise time measurements, while for optical efficiency measurements, a large area detector was used as a PIN photodiode S3588-09 from HAMAMATSU (active area of 3 mm × 30 mm) with a custom-built TIA amplification stage.

Finally, an optical fiber spectrometer from AVANTES (AVASPEC-mini2048CL-UVI25) was used for spectral measurements. The excitation laser source used in all experimental measurements was the LP405C1 from THORLABS, with a wavelength of 405 nm. The optical modulation was achieved using a BIAS-T driven by an arbitrary waveform generator from SIGLENT (SDG703A) with a square wave at 5 MHz. All measurements were performed with a lateral scan on the FC, translating the laser spot (1 mm in diameter). At each spot position, the rise time, the optical

Table S1. FLIM fit results for LR305 and DQ1 FCs. LR305 measured at 40 MHz (mono-exponential), DQ1 at 20 MHz (bi-exponential). τ in ns, χ^2 goodness of fit, τ_{av} amplitude-weighted average lifetime for bi-exponential fits.

Dye	Conc.	Fit Type	A_1	τ_1	A_2	τ_2	χ^2	τ_{av}
LR305	750 ppm	mono-exp	-	5.20	-	-	0.983	5.20
	$(9 \cdot 10^{-4} M)$	mono-exp	-	5.35	-	-	1.039	5.35
		mono-exp	-	5.19	-	-	1.081	5.19
	1000 ppm	mono-exp	-	5.35	-	-	1.102	5.35
	$(1.21 \cdot 10^{-3} M)$	mono-exp	-	5.25	-	-	1.171	5.25
		mono-exp	-	5.35	-	-	1.090	5.35
DQ1	500 ppm	bi-exp	1623	8.01	1942	5.20	0.977	6.5
	$(8 \cdot 10^{-4} M)$	bi-exp	1205	8.10	1328	5.00	1.021	6.4
		bi-exp	1798	7.90	1743	5.10	1.043	6.5
	750 ppm	bi-exp	1520	7.70	1099	4.90	1.017	6.6
	$(1.2 \cdot 10^{-3} M)$	bi-exp	1322	7.90	1002	4.60	1.109	6.4
		bi-exp	2950	7.70	1947	4.60	1.046	6.5

efficiency and the emission spectrum were acquired. In all measurements, data acquisition was performed using the KEYSIGHT DSOX6004A oscilloscope.

The experimental setup used for the measurements is shown in Fig.S2a.

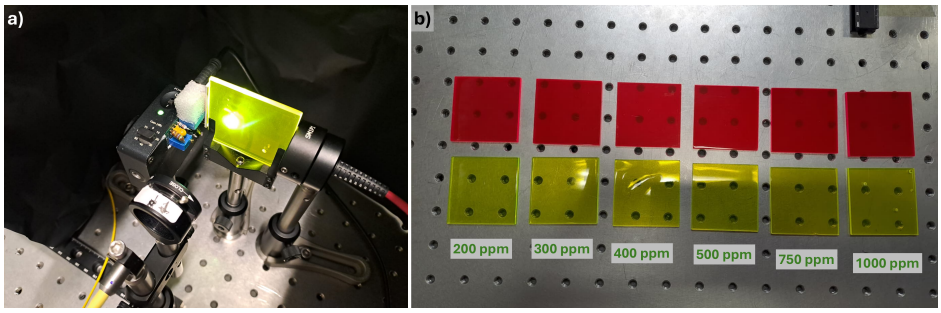

Fig. S2. Left: Experimental setup used for the measurements;Right: Samples analyzed during the experimental characterization, embedding LR305 (red samples) or DQ1 (yellow samples) as fluorophore in the concentrations reported below.

F. Summary of experimental parameters

Table S2 reports a summary of the experimental parameters used in the Monte Carlo simulations.

2. MONTE CARLO METHOD

All simulations were performed on a Windows 10 Pro workstation equipped with an Intel® Xeon® E-2146G CPU (6 physical cores, 12 logical cores, 3.50 GHz) and 16 GB RAM. MATLAB R2019a [1] was employed for numerical computations, with parallelization configured to utilize all 12 logical cores, though only 6 were actively used due to hyper-threading constraints.

The Monte Carlo code was developed in-house using `PVTrace` [2] as the foundational framework. Several custom subroutines were integrated to enable time-dependent modeling and to adapt the simulation to the specific characteristics of our FC system.

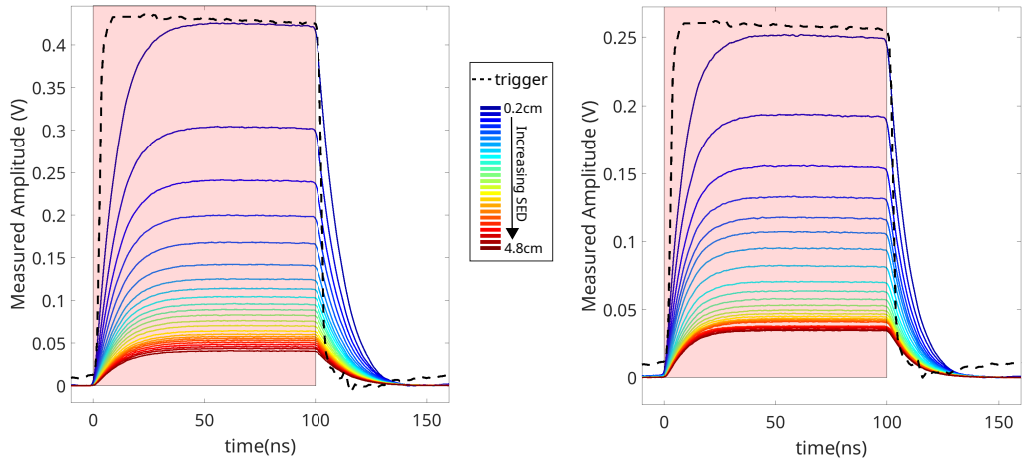

Fig. S3. Signal amplitude recorded as a function of time at different SEDs (solid lines) in case of LR305 (left) and DQ1 (right) filled slabs. Trigger (dashed black line) used to modulate the laser source emission. The red area in the background indicates the simulated time interval.

LR305 series					**DQ1 series**				
conc (ppm)	conc (M)	QY (%)	Thickness (mm)	τ (ns)	conc (ppm)	conc (M)	QY (%)	Thickness (mm)	τ (ns)
200	$2 \cdot 10^{-4}$	84.8	2.78	5.3	200	$3 \cdot 10^{-4}$	85.8	3.07	6.4
300	$4 \cdot 10^{-4}$	86.0	2.84	//	300	$5 \cdot 10^{-4}$	86.9	2.72	//
400	$5 \cdot 10^{-4}$	87.2	2.69	//	400	$6 \cdot 10^{-4}$	90.1	2.78	//
500	$6 \cdot 10^{-4}$	82.6	2.72	//	500	$8 \cdot 10^{-4}$	84.3	2.83	//
750	$9 \cdot 10^{-4}$	81.7	3.08	//	750	$1.2 \cdot 10^{-3}$	87.3	2.71	//
1000	$1.2 \cdot 10^{-3}$	79.7	3.07	//	1000	$1.5 \cdot 10^{-3}$	88.4	2.85	//

Table S2. Optical and physical properties of LR305 and DQ1 filled slab at different dye concentration.

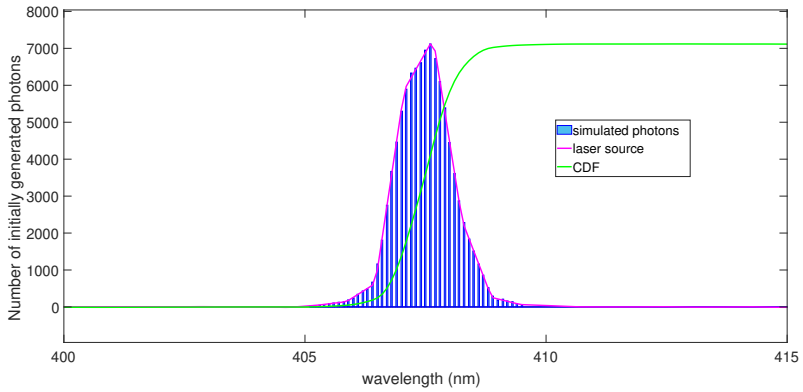

Fig. S4. Experimentally measured laser source spectra (violet line) and CDF (green line), histogram of randomly generated photons as a function of wavelength used in the Monte Carlo simulation

.

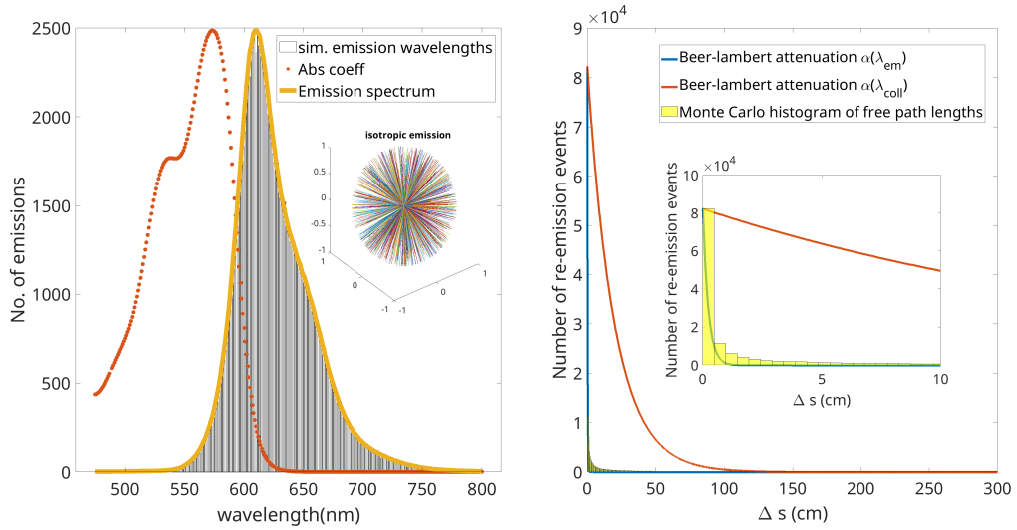

Fig. S5. Simulation of LR305 slab, 500 ppm ($6 \cdot 10^{-4} M$), 2.5 SED. Left: Histogram of simulated wavelengths of photons emitted after reabsorptions; Normalized absorption (red dots) and fluorescence (yellow line); the good agreement between the histogram and the fluorescence curve in yellow confirms the consistency between the stochastic sampling method and the expected emission distribution; The inset shows simulated directions of emitted photons, showing isotropic emission. Right: distribution of photon free path lengths within the FC slab. The yellow histogram represents the Monte Carlo–generated free path lengths at each reabsorption/re-emission event. The overlaid curves correspond to the Beer–Lambert exponential attenuation law, calculated using the absorption coefficients at (blue line) the mean emission wavelength ($\alpha(\lambda_{em})$), and (red line) the collection wavelength at the FC edge($\alpha(\lambda_{coll})$). Both curves are normalized to the maximum of the histogram. The agreement between the histogram and Beer–Lambert attenuation at λ_{em} (blue line) confirms the consistency between the stochastic sampling method and the expected exponential distribution. The Beer–Lambert attenuation at λ_{coll} (red line) indicates that collected photons are red-shifted with respect to stationary fluorescence distribution due to self-absorption ($\alpha_{coll} \leq \alpha_{em}$).

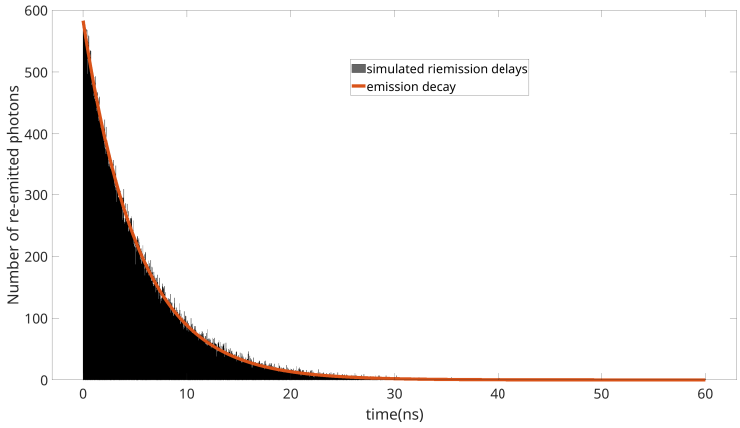

Fig. S6. Distribution of simulated re-emission times after reabsorptions, in case of a simulation of LR305 slab (500 ppm - $6 \cdot 10^{-4} M$, 2.5cm SED). The red curve represents the emission decay curve considering a lifetime of LR305 of 5.3 ns. The good agreement between the histogram and the decay curve in red confirms the consistency between the stochastic sampling method and the expected time distribution

A. ray-plane intersection routine

The ray-plane intersection routine, schematized in Fig. S7, is used to evaluate the interaction face and the coordinates of the interaction point $\mathbf{P_{int}}$: each photon segment was defined by its start and end points, $\mathbf{P}_0$ and $\mathbf{P}_1$, respectively, and each FC surface was represented as a plane defined by a known point $\mathbf{P}_3$ on the plane and the surface normal unit vector $\hat{\mathrm{n}}$. The intersection parameter r along the photon segment was computed as

$$r = \frac{(\mathbf{P}_3 - \mathbf{P}_0) \cdot \hat{\mathrm{n}}}{(\mathbf{P}_1 - \mathbf{P}_0) \cdot \hat{\mathrm{n}}}, \tag{S1}$$

If $0 \leq r \leq 1$, an intersection between the photon segment and the considered surface occurs along the segment. The actual intersection coordinates were then obtained using the parametric line equation

$$\mathbf{P}_{\mathrm{int}} = \mathbf{P}_0 + r(\mathbf{P}_1 - \mathbf{P}_0). \tag{S2}$$

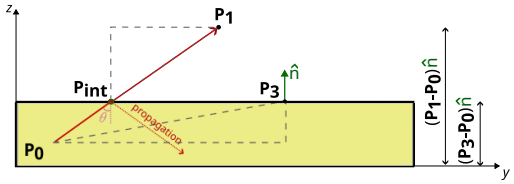

Fig. S7. 2D projection scheme of the geometric configurations in the Monte Carlo routine to find out whether the propagated photons encounter a slab interface and to compute the interaction coordinates $\mathbf{P_{int}}$. $\mathbf{P_0}$ and $\mathbf{P_1}$ are the coordinates of initial emission and end point of the simulated free path, respectively. $\mathbf{P_3}$ is an arbitrary point on the surface.

To ensure that the photon intersected the physical surface rather than an extension of the plane, the intersection point was further checked against the rectangular bounds of the FC slab. If $\mathbf{P}_{\mathrm{int}}$ lays within these limits, the photon was considered to have interacted with the surface, allowing for reflection, transmission, or escape. This procedure was applied iteratively to all faces of the FC, providing a robust geometric inclusion test consistent with the Monte Carlo propagation framework.

B. Time-behavior simulation

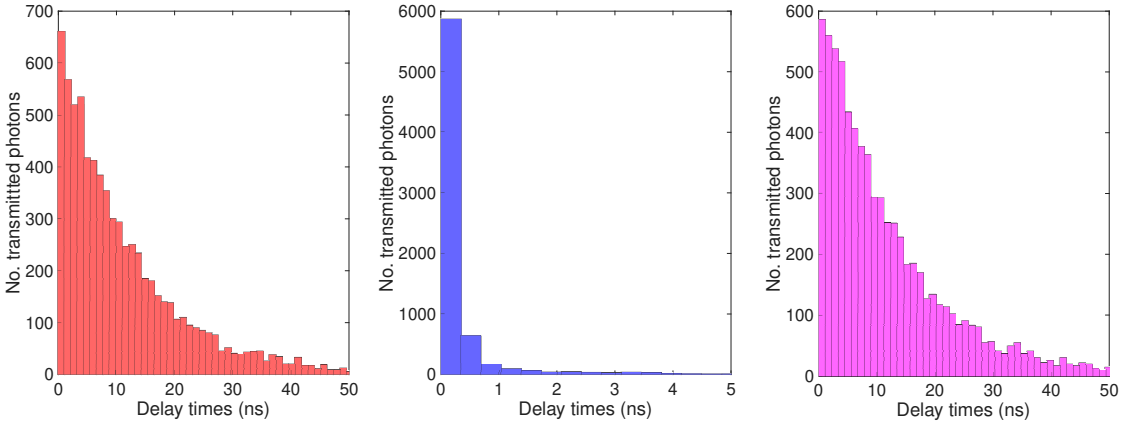

Fig. S8. Histograms (relative to simulations on LR305 filled slab, 500 ppm -6 · $10^{-4}M$, 2.5cm SED) showing the different contribution to the arrival time of the photons to the detector: delays due to emission lifetime (left), due to optical path (center) and total cumulated delay (right).

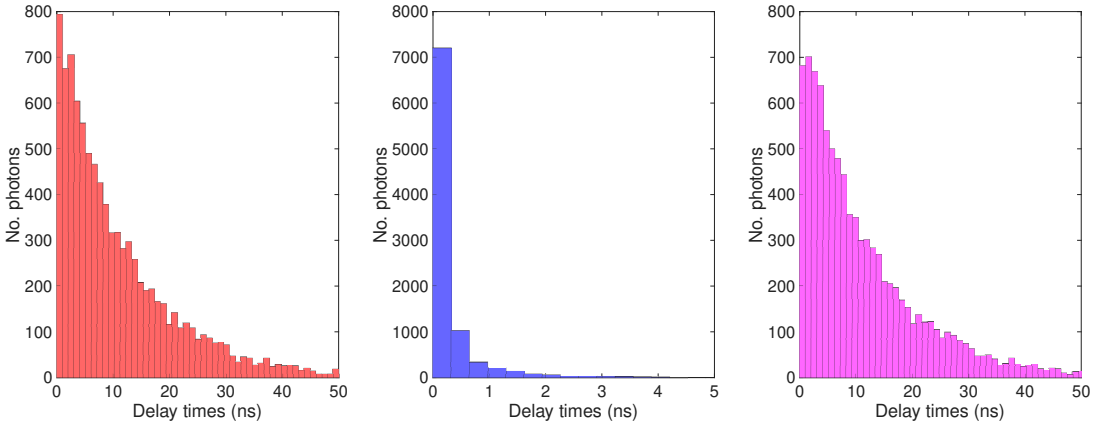

Fig. S9. Histograms (relative to simulations on DQ1 filled slab, 400 ppm - 6 · $10^{-4}M$, 2.5cm SED) showing the different contribution to the arrival time of the photons to the detector: delays due to emission lifetime (left), due to optical path (center) and total cumulated delay (right).

3. MONTE CARLO SIMULATIONS: REABSORPTIONS

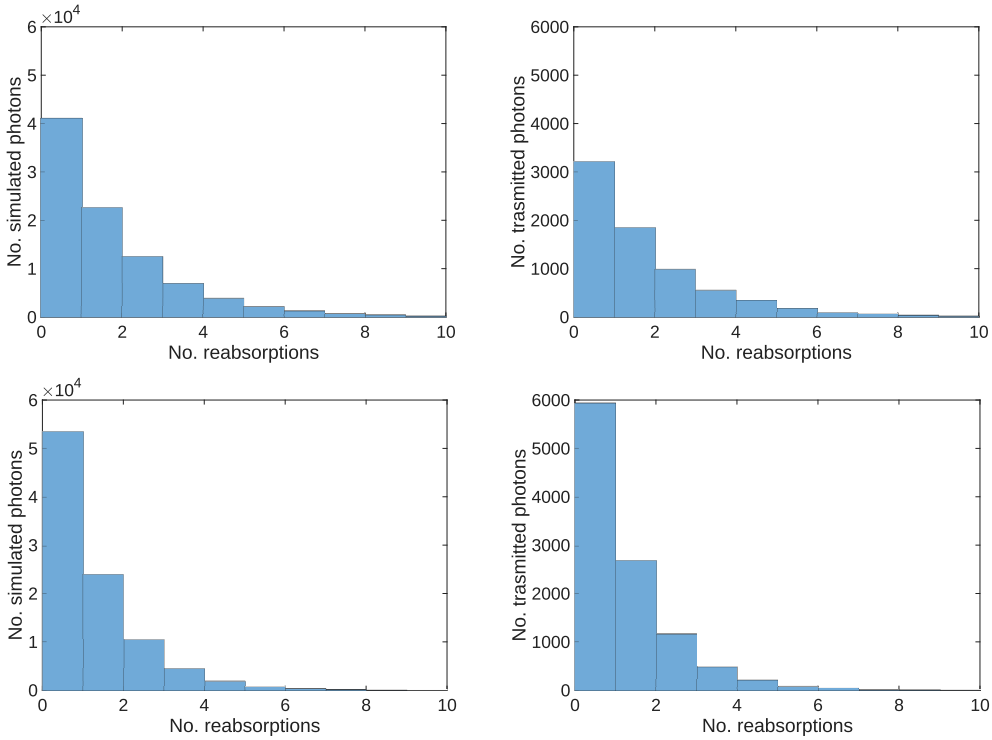

Fig. S10. Histogram of number of reabsorptions events during the photons trajectories (left - total simulated, right - ending in face transmission), in case of simulations of LR305 (top) and DQ1 slab (bottom), both $6 \cdot 10^{-4} M$ (500 ppm for LR305 and 400 ppm for DQ1), and 2.5 cm SED.

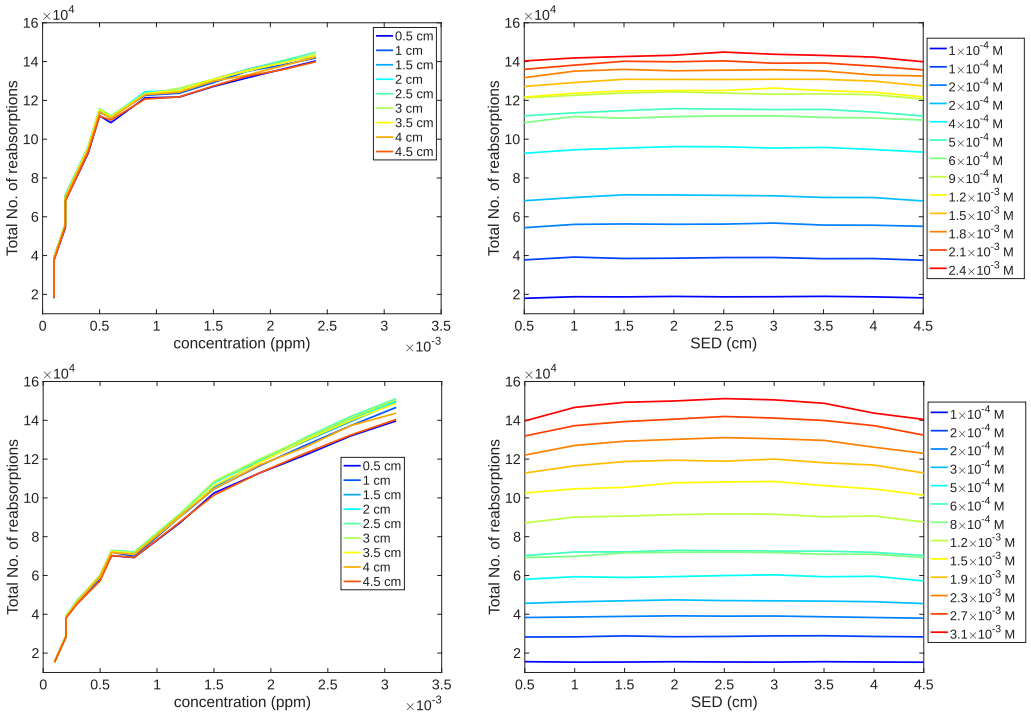

Fig. S11. Left: Total number of reabsorption events per transmitted photons as a function of concentration and at different SED, in case of LR305-filled slab (top) and DQ1-filled slab (bottom). Right: Total number of reabsorption events as a function of SED and at different concentrations, in case of LR305-filled slab (top) and DQ1-filled slab (bottom).

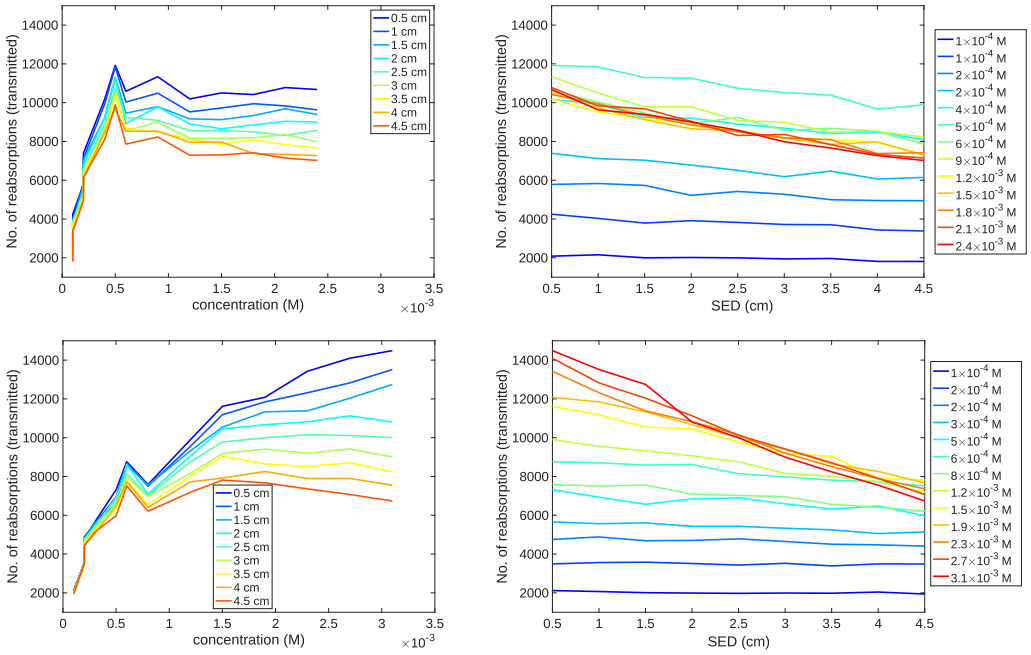

Fig. S12. Left: Number of reabsorption events (counted on trajectories that ends in transmission through face coupled with detector) per transmitted photons as a function of concentration and at different SED, in case of LR305-filled slab (top) and DQ1-filled slab (bottom). Right: Number of reabsorption events (counted on trajectories that ends in transmission through face coupled with detector) as a function of SED and at different concentrations, in case of LR305-filled slab (top) and DQ1-filled slab (bottom).

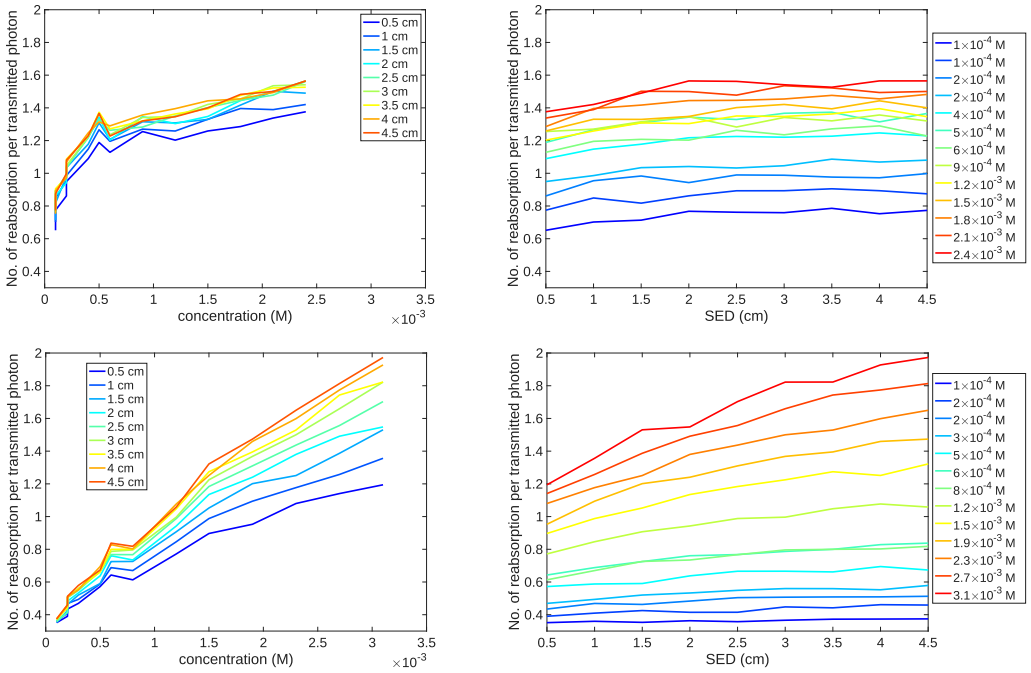

Fig. S13. Left: Average number of reabsorption events per transmitted photons as a function of concentration and at different SED, in case of LR305-filled slab (top) and DQ1-filled slab (bottom). Right: Average number of reabsorption events as a function of SED and at different concentrations, in case of LR305-filled slab (top) and DQ1-filled slab (bottom).

4. MONTE CARLO SIMULATIONS: EFFICIENCY

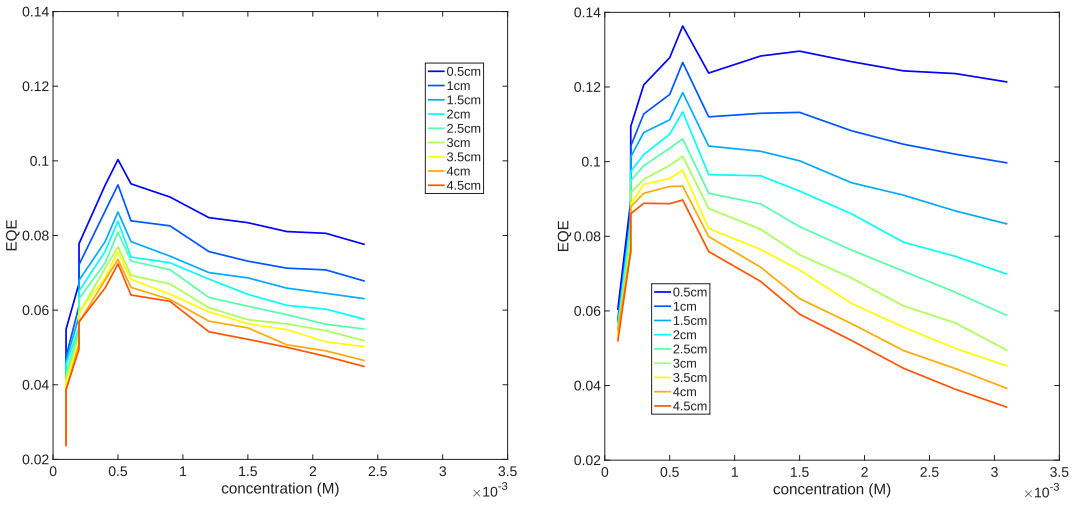

Fig. S14. Simulated external quantum efficiency (EQE) as a function of concentration in case of LR305 (left) and DQ1 (right) filled slabs for various source to detector distances (SEDs)

5. MONTE CARLO SIMULATIONS: TIME RESPONSE

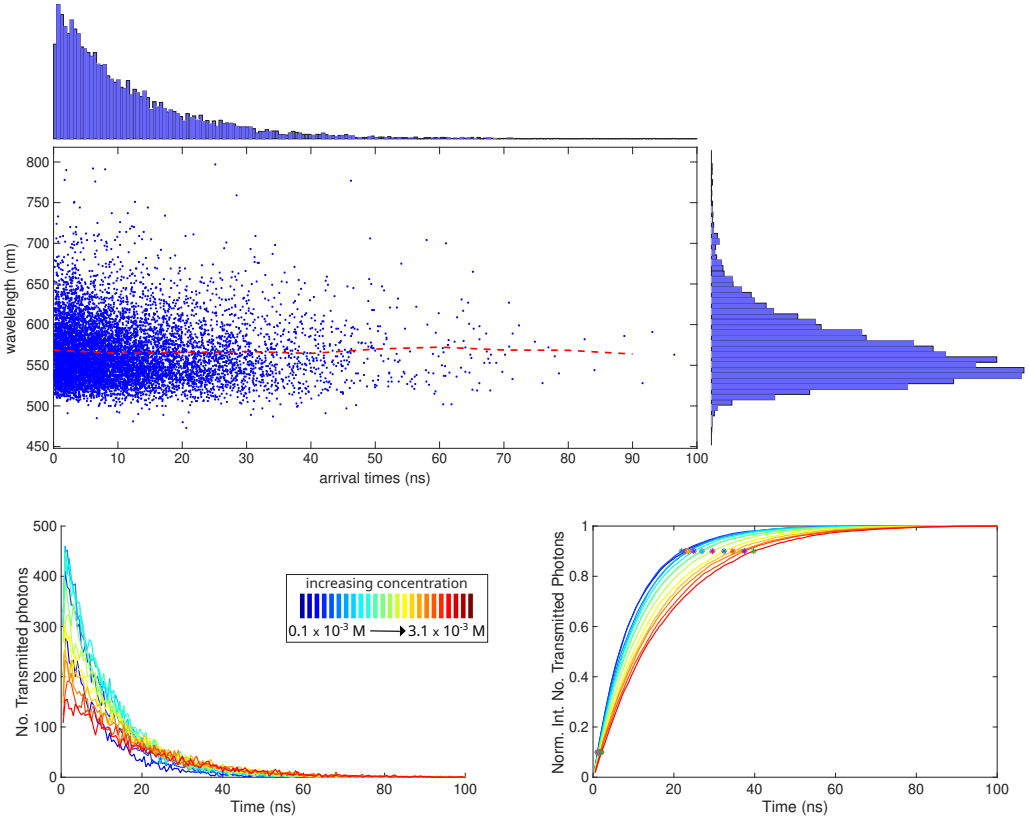

Fig. S15. Top: bidimensional scatter plot of photons transmitted from the slab face coupled with the detector, as a function of arrival times and wavelength (from simulation of DQ1 filled slab @ 2.5 cm SED, 400 ppm - $6 \cdot 10^{-4} M$); Corresponding histograms of arrival times and photons wavelength are shown on top and right side, respectively. Bottom: Number of photons transmitted from slab edge as a function of arrival times (response to an instantaneous laser pulse), extracted from simulations of DQ1 slab at different concentrations and at fixed SED of 2.5cm (left); Normalized Integrated number of photons computed from left panel in order to simulate the response to a finite-size square laser pulse (right).

6. REPEATABILITY ANALYSIS OF SIMULATIONS

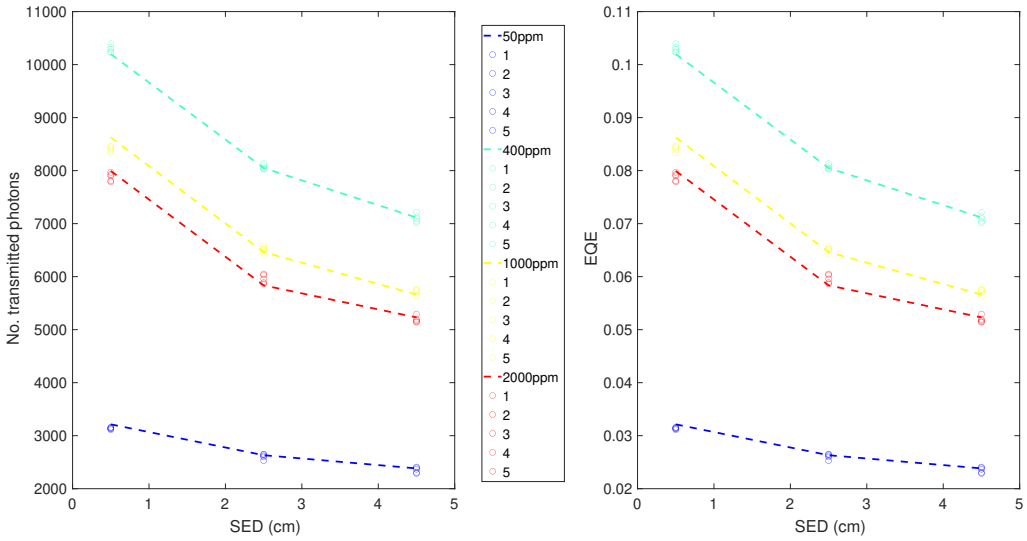

Fig. S16. Repeatability study of LR305 filled slab: results of 5 identical simulations (repeated at selected SED and concentrations). LEFT: No. of transmitted photons from F1 face (circles) as a function of source-to-edge distance and at different concentrations. The dashed line is extracted from the main simulation discussed in the paper. RIGHT: EQE (circles) as a function of source-to-edge distance and at different concentrations. The dashed line is extracted from the main simulation discussed in the paper.

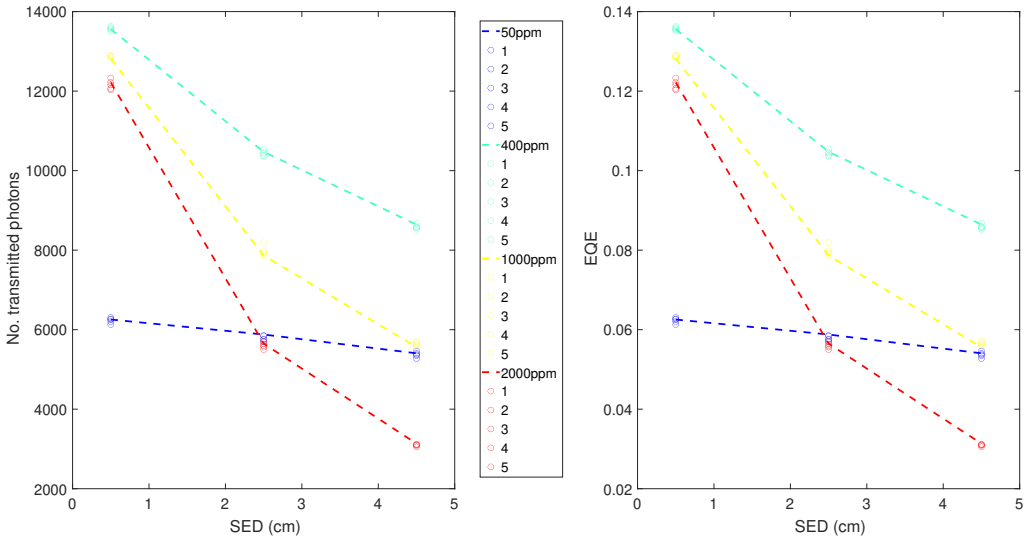

Fig. S17. Repeatability study of DQ1 filled slab: results of 5 identical simulations (repeated at selected SED and concentrations). LEFT: No. of transmitted photons from F1 face (circles) as a function of source-to-edge distance and at different concentrations. The dashed line is extracted from the main simulation discussed in the paper. RIGHT: EQE (circles) as a function of source-to-edge distance and at different concentrations. The dashed line is extracted from the main simulation discussed in the paper.

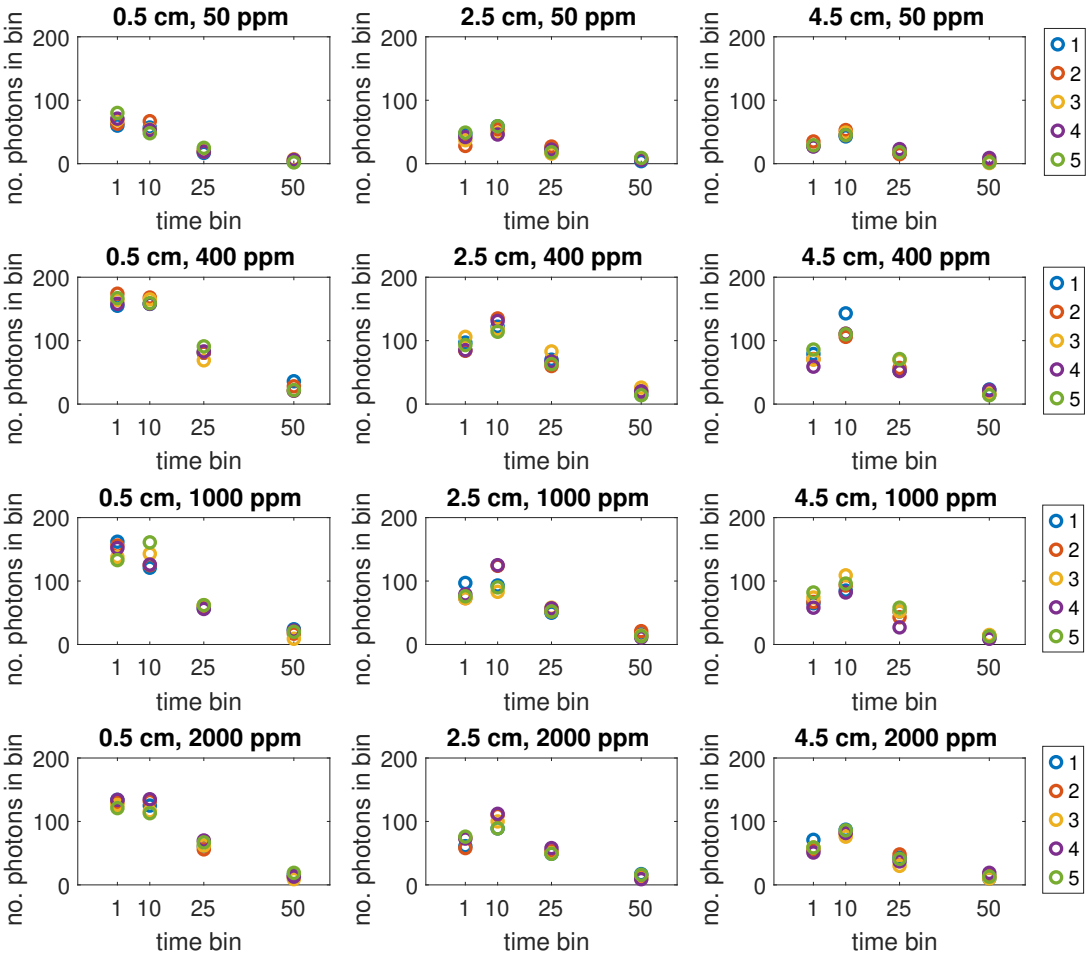

Fig. S18. Repeatability study of LR305 filled slab: results of 5 identical simulations (repeated at selected SED and concentrations). Number of transmitted photons in selected temporal bins, used to extract the FC time response.

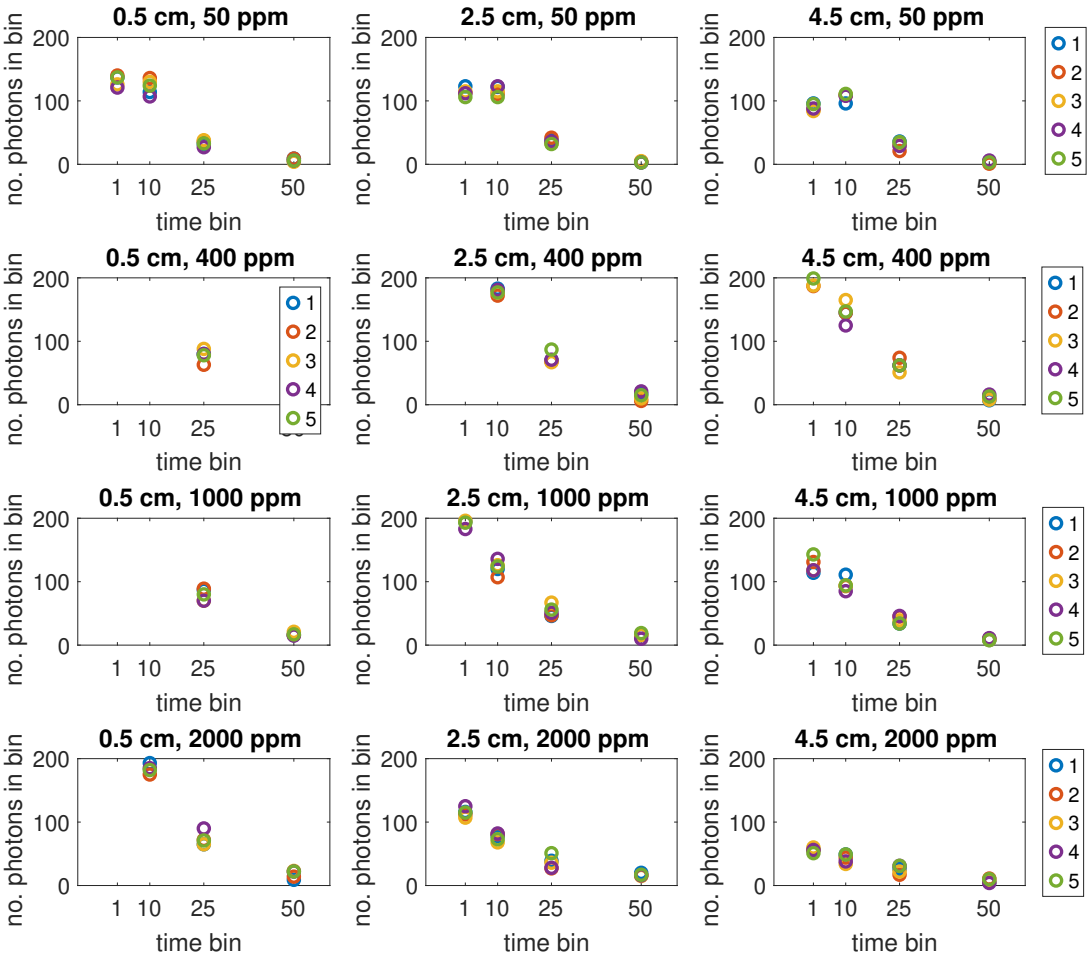

Fig. S19. Repeatability study of DQ1 filled slab: results of 5 identical simulations (repeated at selected SED and concentrations). Number of transmitted photons in selected temporal bins, used to extract the FC time response.

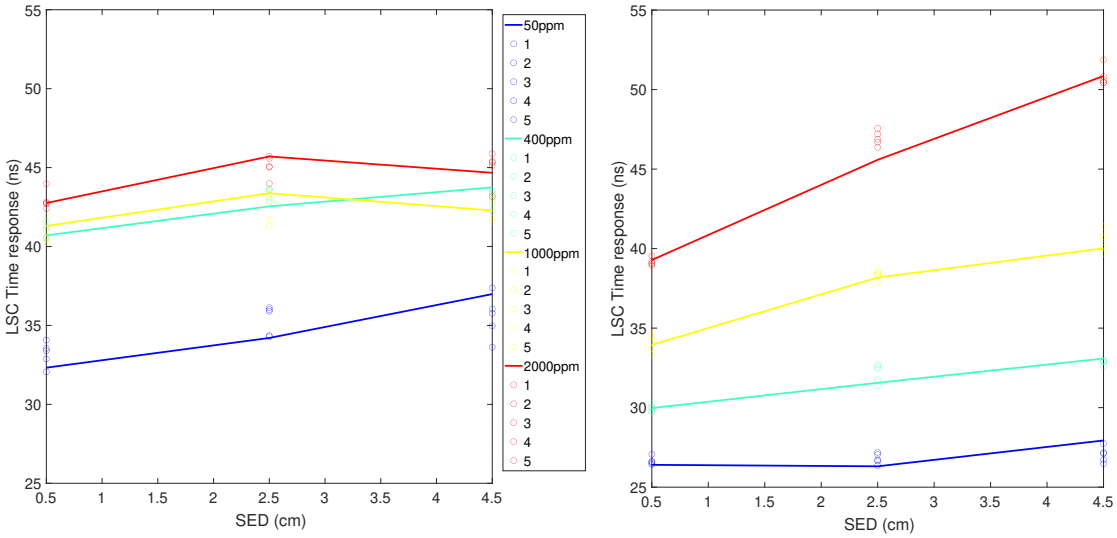

Fig. S20. Repeatability study of LR305 (LEFT) and DQ1 (RIGHT) filled slab: results of 5 identical simulations (repeated at selected SED and concentrations): FC time response (circles) as a function of source-to-edge distance and at different concentrations. The dashed line is extracted from the main simulation discussed in the paper.

7. COMPARISON WITH EXPERIMENTS

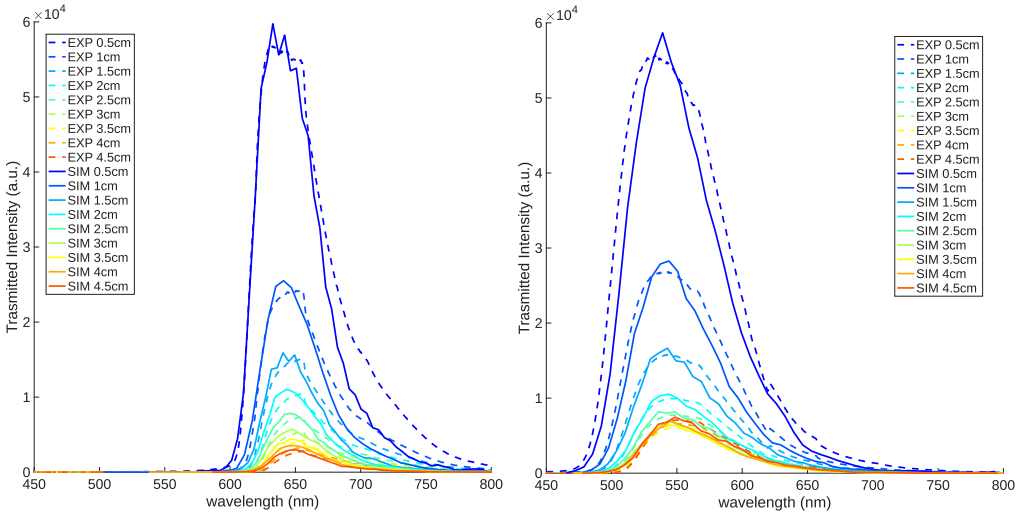

Fig. S21. Simulated (solid lines) and experimental (dashed lines) spectra of collected photons as a function of concentration in case of LR305 (left) and DQ1 (right) filled slab at different SED and $6 \cdot 10^{-4} M$ (500 ppm for LR305 and 400 ppm for DQ1).

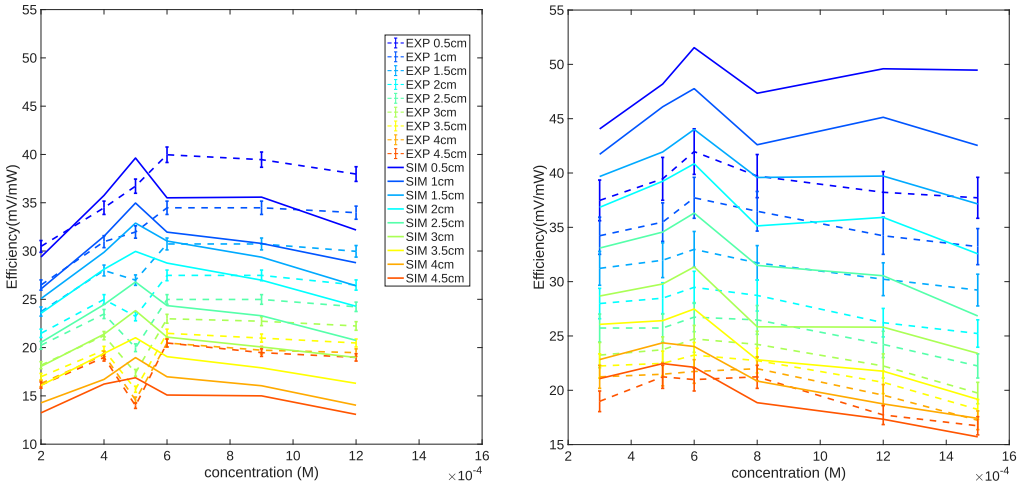

Fig. S22. Simulated (solid lines) and experimental (dashed lines) collection efficiency as a function of concentration in case of LR305 (left) and DQ1 (right) filled slab at different SED.

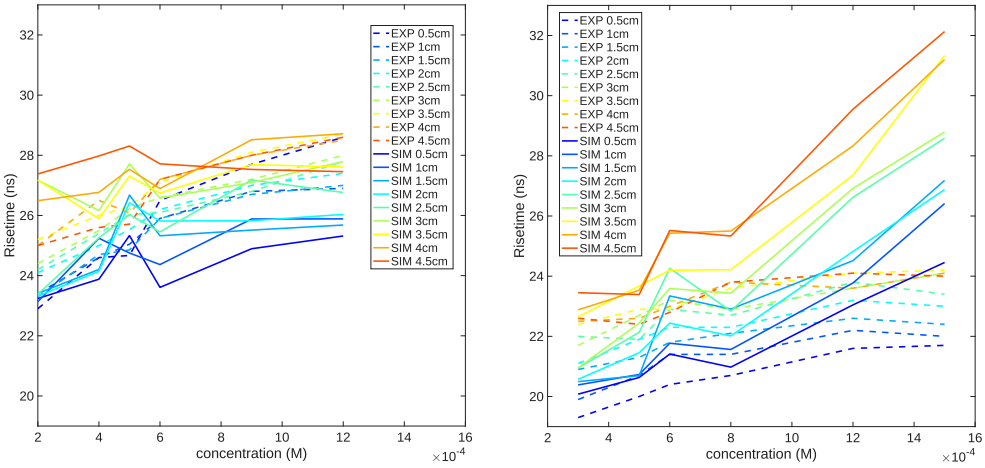

Fig. S23. Simulated (solid lines) and experimental (dashed lines) Rise time as a function of concentration in case of LR305 (left) and DQ1 (right) filled slab at different SED.

REFERENCES

1. The MathWorks, Inc., *MATLAB, Version R2019a*, Natick, Massachusetts, USA (2019), available at https://www.mathworks.com.
2. D. J. Farrell, *Pvtrace: Optical Ray Tracing for Luminescent Materials and Spectral Converter Photovoltaic Devices*, GitHub repository (2021), available at https://github.com/danieljfarrell/pvtrace, accessed January 13, 2021.